Monthly Notices of the ROYAL ASTRONOMICAL SOCIETY

MNRAS **502,** 5362–5369 (2021) doi:10.1093/mnras/stab080

Stability time-scale prediction for main-belt asteroids using neural networks

Chao Liu,★ Shengping Gong ★ and Junfeng Li

School of Aerospace Engineering, Tsinghua University, Beijing 100084, China

Accepted 2021 January 1. Received 2021 January 1; in original form 2020 May 10

ABSTRACT

Many asteroids move in the belt between the orbits of Mars and Jupiter under the gravitational attraction of the Sun and planets in the Solar system. If one of these asteroids does not leave the belt during a period, it is considered to be temporarily stable on that time-scale. This paper aims to study the time-scales on which asteroids could stay in the main belt. A simplified situation is studied in which the initial orbital inclinations and the longitudes of the ascending nodes of the asteroids are set to zero. Numerical integration is used to study the temporal stability of the main-belt asteroids. In the integration, the distribution of the instability time for randomly generated particles can be fitted with a function. Thus a reasonable method is presented to choose an integration time-scale based on the percentage of the already unstable particles in relation to all unstable particles. A total of 151 000 particles are generated and then integrated for 8.09×10^6 yr. The integration data are used to train the probabilistic neural networks to predict the stability of particles. A temporal stability map in the *a*-*e* plane is obtained from the prediction results of the neural networks.

Key words: methods: numerical – celestial mechanics – minor planets, asteroids: general.

1 INTRODUCTION

Asteroids are minor planets orbiting the Sun, and they are key to our understanding of the origin and evolution of the Solar system. Nearly a million asteroids have been detected so far. Most of the asteroids detected are those with larger diameters. The known asteroid size distribution implies that there is an undetected population of an estimated 10^{13} asteroids with diameters larger than 1 m (Bottke et al. 2005). Except for the interesting near-Earth asteroids (Alessio & Dario 2018; Jopek 2020), a large proportion of the detected asteroids move in the main asteroid belt, which is the region between the orbits of Mars and Jupiter. These are categorized as main-belt asteroids.

The dynamics of the main-belt asteroids are of great interest to researchers. It was over 150 years ago that Daniel Kirkwood discovered main-belt gaps at certain values of the semimajor axis. They clearly show that there is a lack of asteroids in concordance with the 4/1, 3/1, 5/2, 7/3 and 2/1 mean motion commensurabilities with Jupiter. The search for an explanation of the Kirkwood gaps motivates the study of mean motion resonance dynamics (Moons 1997).

In addition to the Kirkwood gaps, the clustering of the asteroids in the main belt is also a phenomenon worthy of study. Millions of asteroids move in the belt. If some of them escape from the main asteroid belt, they could become Earth-crossers, and potentially pose a great threat to Earth. So it is important to find out how many detected asteroids will escape from the belt and when they will escape. This is the goal of this work. There is no analytical method to answer the problem. Therefore, at the moment, numerical integration is the only available method.

With advances in computer performance, numerical methods have been widely used for problems that cannot be solved analytically. Numerical work involves a wide range of simulations of the system. Regarding the general *N*-body problem, research has been devoted to determining the minimum of the initial semimajor axis difference to avoid close encounters. Most studies focused on the three-body system (Harrington 1972; Donnison & Mikulskis 1992, 1994), while some tackled the four-body system (Chambers, Wetherill & Boss 1996; Duncan & Lissauer 1997; Faber & Quillen 2007; Smith & Lissauer 2009; Obertas, Van Laerhoven & Tamayo 2017). In particular, Tamayo et al. (2016) provided a method to predict the stability of tightly packed planetary systems using optimized machine-learning classifiers.

In relation to the main asteroid belt, numerical methods have been applied to explain the formation of the Kirkwood gaps. Wisdom (1982, 1983) found that in the planar elliptic restricted three-body problem, a test particle at the 3/1 resonance can spend 100 000 yr or longer with $e < 0.1$ and then jump suddenly to $e > 0.3$. Thus the particle becomes a Mars-crosser and could be swept by a collision with Mars. Gladman et al. (1997) carried out numerical simulations of particles placed in orbital resonances in the main asteroid belt to estimate their dynamical lifetimes and the transport mechanism to the region of the terrestrial planets. Other works have investigated the transport from the main belt to the near-Earth region or other regions (Novaković et al. 2015; Hsieh et al. 2020).

Secular resonances with and perturbations by the major planets or massive asteroids also play an important role in the dynamics of the main-belt asteroids (Carruba, Vokrouhlický & Novaković 2018; Milani et al. 2010; Minton & Malhotra 2010; Novaković et al. 2015).

★ E-mail: 18010128321@163.com (CL); gongsp@tsinghua.edu.cn (SG)

Todorović & Novaković (2015) used the fast Lyapunov indicator (FLI) to produce a stability map in the part of the main-belt region where the Pallas asteroid family is located.

The formation of the main asteroid belt is also an interesting topic that has been intensively studied. The work of Minton & Malhotra (2009, 2011) shows that it is impossible to reproduce the current situation in the asteroid belt within the current architecture of the Solar system. The simulated asteroid belt after integration for 4×10^9 yr does not match the observed main-belt asteroids in the semimajor axis distribution. On the other hand, once the migration of the giant planets is taken into account, the distribution of the simulated asteroid belt matches that of the observed belt well. Other studies have been carried out to investigate the orbital distribution of the main asteroid belt (Roig & Nesvorný 2015; Deienno et al. 2016; Malhotra & Wang 2016; Clement et al. 2018, 2019).

Granvik et al. (2017) investigated the escape routes from the main belt, and more than 10 obvious escape routes have been found. Beyond that, few works have focused on the evolution of the main-belt asteroids within the current structure of the Solar system. Moreover, there is no criterion for choosing the time-scale of an integration. In previous numerical works, the time-scale was usually chosen based on the computing capacity at the time, for example 10–20 revolutions of the outer orbit (Harrington 1972), 1000 inner orbits (Donnison & Mikulskis 1992), 10^4 binary periods (Holman & Wiegert 1996), or 10^7 inner orbits (Tamayo et al. 2016). These time-scales cannot guarantee that the systems (or particles) that are stable during the integrations will still be stable when it comes to a longer simulation. As in the numerical work, an asteroid could behave stably in the integration of a short time-scale but unstably on a longer time-scale. However, the time at which the asteroid begins to be unstable is unknown, and it is impossible to integrate for infinite time. Thus a reasonable time-scale is one of the keys to obtaining a reliable result. The criterion to determine the integration time-scale needs to be established first.

On the one hand, it is very difficult to integrate all the main-belt asteroids with a long time-scale. Even if this were done, the integration would need to be carried out again for newly detected asteroids. On the other hand, if we follow the traditional numerical methods, our work can be carried out by integrating many asteroids and sketching the border of the stable region. There are six degrees of freedom of the asteroids. If each degree is divided into 20 parts, 20^6 asteroids need to be integrated to obtain a rough border. This is much higher than the number of detected main-belt asteroids. Otherwise, many simplifications have to be made, such as setting the initial orbital elements except the semi-major axes and eccentricities of the asteroids to be zero. This makes the result poorly applicable. The stable and unstable regions are mixed up because of the complex dynamics of the main-belt asteroids. Thus the mixed regionsincreases the difficulty of sketching the border and then makes the application more difficult.

Machine learning provides a valid method to handle these problems. Smirnov, Dovgalev & Popova (2018) used an improved automatic identification algorithm to identify all asteroids in three-body mean motion resonances. Tamayo et al. (2016) were the first to present a new machine-learning approach to predict the stability of tightly packed planetary systems. The use of a neural network means that few simplifications need to be made. In addition, the neural network can be trained with relatively fewer data. After the training, the stability of a given asteroidcan be predicted by the neural network immediately.

This paper is devoted to studying the temporal stability of the main-belt asteroids using numerical integration. First of all, a reasonable method is presented to choose the time-scale of an integration. The time-scale is determined based on the percentage of the already unstable particles in relation to all unstable particles. After that, a simulation of 151 000 particles is carried out, and the results are applied to training the probabilistic neural network. Thus the stability of asteroids in the belt can be predicted rapidly and accurately.

2 ASSUMPTION OF TEMPORAL STABILITY

The main asteroid belt is a region in our Solar system located roughly between the orbits of the planets Mars and Jupiter. How long an asteroid will stay in the belt is the quantity to be determined. In the model, the Sun and eight planets move under their mutual gravitational attraction. All the massive bodies are considered to be point masses, and the gravitational effects from bodies out of the model are ignored. Forces of non-gravitational origin are also ignored, such as the Yarkovsky effect (Bottke et al. 2006; Delbo' et al. 2007; Yan & Li 2019), because of the very long periods of such effects.

Asteroids in the main asteroid belt are assumed to be massless and only to be perturbed by and interact with massive bodies during the simulation. Hence, asteroids do not perturb one another, nor collide with each other, but collisions between an asteroid and the massive bodies are allowed.

If the asteroid does not leave the main asteroid belt during a period, it is considered to be temporarily stable on this time-scale. For the benefit of discussion, the assumption of temporal stability is given as follows.

In the Solar system, there is a belt between the planets Mars and Jupiter in the range of ($r_{\rm min}$, $r_{\rm max}$) with respect to the distance from the Sun. Here

$$r_{\rm min} = a_{\rm M}(1 + e_{\rm M}), \quad r_{\rm max} = a_{\rm J}(1 - e_{\rm J}), \tag{1}$$

where $a_{\rm M}$ and $a_{\rm J}$ are the semimajor axes of Mars and Jupiter respectively, and $e_{\rm M}$ and $e_{\rm J}$ are the eccentricities. An asteroid moves in the belt under the gravitation of the Sun and eight planets. During a period of time, T, if it does not escape, the asteroid is considered to be *temporarily stable* on the time-scale T. If it escapes from the belt, the asteroid is *unstable* on the time-scale T. The longest time that an asteroid can stay in the belt is termed its *instability time*.

3 TIME-SCALE OF INTEGRATIONS

Numerical simulations are carried out using the Hybrid symplectic integrator in the MERCURY integrator package (Chambers & Migliorini 1997). The symplectic integrator is very fast but moderately accurate. Because neural network training requires a lot of data, it is more appropriate to use the Hybrid symplectic integrator.

After defining the temporal stability and selecting the integrator, the time-scale needs to be determined before the integration. It is mostly computational costs that limit the number of test particles and the time-scale of integration. In previous works, different magnitudes of the time-scale were chosen based on the computing capacity at the time. These time-scales cannot guarantee that the particles behaving stably during the integration will still be stable when it comes to a longer simulation. At the end of the integration, the surviving particles could be unstable, and the proportion of unstable particles in these surviving particles is uncertain.

Our method to determine an appropriate integration times-span is as follows. First, we randomly generate a set of asteroids with initial orbits in the belt. The motions of these asteroids are then integrated for 10^6 yr. Next, the integrations are divided into equal

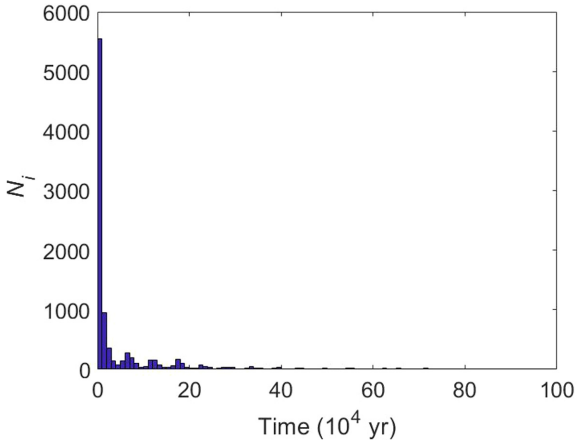

Figure 1. The distribution of the asteroid instability time.

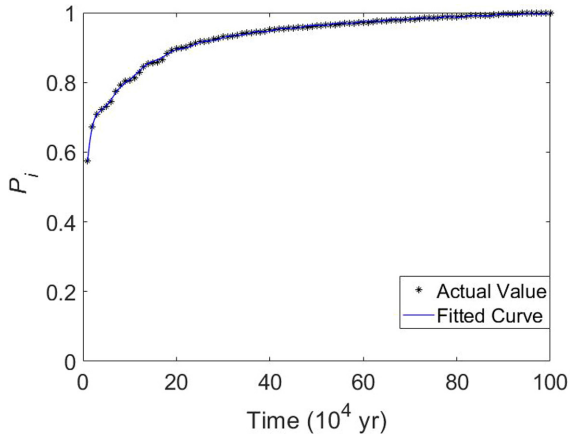

Figure 2. The vertical coordinate $P_i = \sum_{j=1}^{i} N_j/N_{\rm u}$, where $N_{\rm u}$ is the total number of unstable particles.

time intervals, and for each interval the number of unstable asteroids is counted. Finally, the time distribution of the unstable asteroids is fitted with an appropriate function. This function predicts the number of unstable asteroids in an extended time interval and can be used to set the desired integration time-scale.

3.1 Distribution of instability time

For simplicity, the particles are generated with initial orbits in the same plane. The orbital inclinations of the particles are set to zero, as are the longitudes of the ascending nodes. Thus the six degrees of freedom for the initial orbital parameters are reduced to four degrees. It should be noted that because the orbits of the eight massive planets are spatial, the particle motions are spatial, too.

The initial time is set at Julian Day 2 458 600, and the initial orbits of the eight planets are given as the orbits at that time. A total of 20 000 particles are generated randomly with initial orbits in the belt. The integrations are carried out for 10^6 yr. During the integrations, some of the particles stay in the belt, so they are considered to be temporarily stable for this integration duration. For the others, the first time at which a particle leaves the belt is recorded as its instability time.

The number of unstable particles in this integration is denoted as $N_{\rm u}$. The results show that $N_{\rm u} = 9669$. The time-scale of the integration is divided into 100 equal intervals, and each interval is 10^4 yr. Then, in each interval, we count the particles whose instability time is located in the interval and denote the numbers as N_i, $i = 1, 2, ..., 100$. Thus the distribution of the asteroid instability time can be obtained, as shown in Fig. 1. In the first interval, $N_1 = 5550$, which means that more than half of the unstable particles become unstable within 10 000 yr. The value of N_i rapidly decreases with increasing time. This phenomenon will be discussed in Section 4, where there are more data on test particles.

In order to establish a procedure to determine a suitable time-span for the numerical integration, we define P_i as $P_i = \sum_{j=1}^{i} N_j/N_{\rm u}$. The values of P_i as a function of time are shown in Fig. 2. The scatter plot of P_i can be fitted with a function. According to the figure, when $i \leq 5$, P_i increases exponentially; when $i > 5$, P_i increases in the form of a power function with oscillation. The form of the fitted function is determined as

$$p(t) = mnt^{n-1}e^{-mt^n} + \frac{a}{(t+b)^c}\left[1 + d\sin(\eta t + \phi)\right] + k, \quad (2)$$

where e is the Napierian base, and m, n, a, b, c, d, η, ϕ and k are the parameters waiting for fitting. The unit of t is 10^4 yr.

The first term of $p(t)$ is called the 2-parameter Weibull function, one of the most widely used lifetime distributions in reliability engineering. Here, the Weibull function performs well in fitting the early part of the particles' lifetime distribution too. The fitting result is shown in Table 1. The value of the residual sum of squares for these parameters is 6.9435×10^{-4}, which means that the fitted function matches the scatters of P_i well.

It should be noted that for particles generated randomly with no simplifications made about the inclinations and longitude ascending nodes, the corresponding distribution of P_i can be fitted in the same form as $p(t)$.

3.2 The ratio of instability

As discussed above, although the time-scale of the integration is 10^6 yr, there are still unstable particles, whose instability times are longer than the time-scale, hidden in the surviving particles. The total number of the particles that will eventually escape from the belt and become unstable is denoted as $N_{\rm ac}$. Of course, $N_{\rm ac}$ is unknown.

For a better description, we introduce a new concept, which is defined as follows.

$N_{\rm ac}$ is the total number of particles that eventually will escape from the belt. At time T, if N_T particles have escaped from the belt, the ratio α, where $\alpha = N_T/N_{\rm ac}$, is termed the *ratio of instability* at time T.

If the ratio of instability at any time is known, it provides a reference to choose the time-scale. In this problem, at $T = 10^6$ yr, we have $\alpha_{\rm u} = N_{\rm u}/N_{\rm ac}$. Thus the distribution of the ratio of instability within 10^6 yr can be obtained as

$$\alpha(t) = \alpha_{\rm u}\, p(t), \quad (3)$$

where $p(t)$ is given by equation (2). It is reasonable to assume that at the time beyond 10^6 yr, the fitted function (3) of the ratio of instability still works. Therefore, when the time goes to infinity, the value of $\alpha(t)$ should go to 1, which means that

$$\lim_{t\to+\infty} \alpha(t) = 1. \quad (4)$$

In addition, from equation (2) and the parameters given in Table 1, it can be found that

$$\lim_{t\to+\infty} p(t) = k = 1.116301. \quad (5)$$

Table 1. Parameters of the fitted function.

m	n	a	b	c	d	η	ϕ	k
17.135703	−1.172267	−0.609276	0.367441	0.358465	−0.011397	1.079268	−0.694983	1.116301

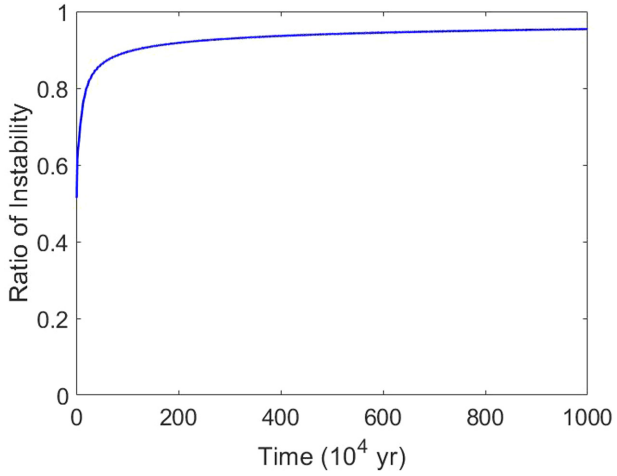

Figure 3. The ratio of instability following the change with time.

Table 2. The value of T for selected values of α.

α	T (10^4 yr)
0.70	8
0.80	20
0.90	117
0.92	216
0.95	809
0.96	1508
0.97	3371
0.98	10456
0.99	72335
0.995	499992

According to equations (3), (4) and (5), we have $\alpha_u = 1/k$. Then $N_{ac} = N_u/\alpha_u = 10\,794$, which means that 53.97 per cent of the particles are unstable.

Then the distribution of the ratio of instability can be rewritten as

$$\alpha(t) = \frac{p(t)}{k}. \quad (6)$$

The ratio of instability against time is shown in Fig. 3. The values of T for selected values of α are listed in Table 2. Now the time-scale of integration can be chosen based on the ratio of instability. If we need the integration results to be more reliable, we can choose a large α such as 0.98, and then the time-scale can be determined according to equation (6).

4 NUMERICAL INTEGRATIONS AND THE TRAINING OF NEURAL NETWORKS

Considering the ratio of instability and the computational cost, we chose the time-scale of 8.09×10^6 yr, at which time $\alpha = 0.95$. A total of 151 000 particles are generated in the belt with initial orbits in the same plane, which means that their inclinations are set to zero, as are the longitudes of the ascending nodes.

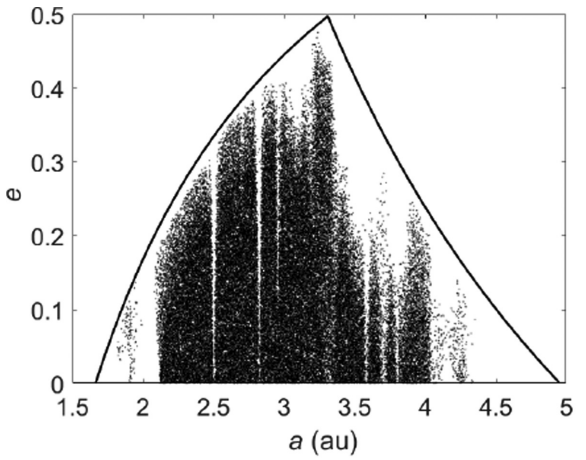

(a) Distribution of stable particles at the start of the integration

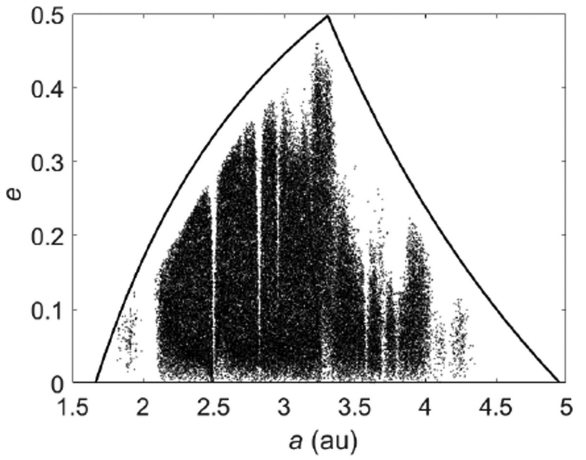

(b) Distribution of stable particles at the end of the integration

Figure 4. The temporarily stable particles in the a-e plane. Here 'au' denotes astronomical units. The solid line is the border of the belt in the a-e plane.

Based on the conclusion drawn in Section 3.2, we can predict the number of particles that will leave the belt during integration. When time goes to infinity, 53.97 per cent of the particles, i.e. 81 495 particles, will escape from the belt. As $\alpha = 0.95$, 95 per cent of them, i.e. 77 420 particles, will become unstable during the integration within 8.09×10^6 yr.

The numerical results show that 81 022 particles become unstable during the integration. The error of the number of the unstable particles between the numerical results and the prediction is about $|77420 - 81022|/77420 = 4.65$ per cent. The stable particles are scattered in the a-e plane, as shown in Fig. 4.

Fig. 3 shows that over half of the unstable particles leave the belt in 10^4 yr. These unstable particles are plotted in Fig. 5(a). They are located close to the borders of the belt or to the most powerful mean motion resonances. The perturbations of the planets drive them to leave the belt in a short time. Of course, some of them just leave temporarily as short-period oscillations of orbits, but they

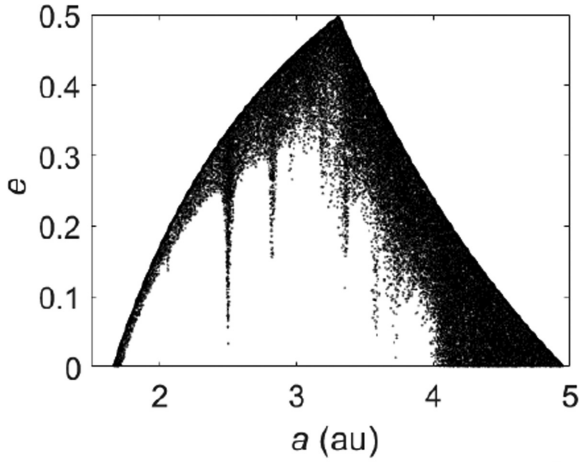

(a) Distributions of the particles leaving the belt within 10^4 yr

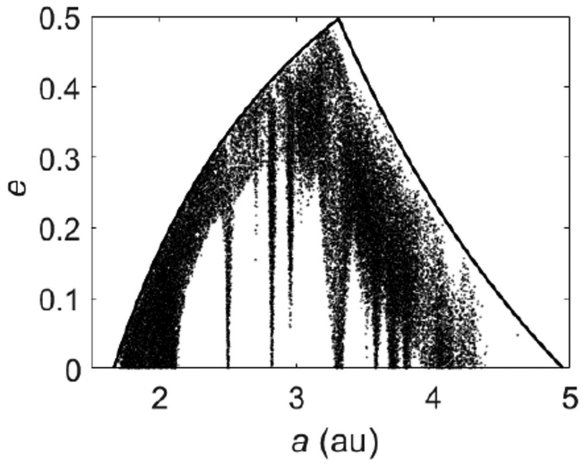

(b) Distributions of the particles leaving the belt after 10^4 yr

Figure 5. The unstable particles with initial orbital elements in the *a*-*e* plane. The solid line is the border of the belt in the *a*-*e* plane.

are also considered to be unstable because collisions may occur. The numerical results also prove that no asteroid near the border survives at the end of the integration.

Compared with Fig. 5(b), the particles near the orbits of Jupiter will be swept up quickly. Most of the particles near the orbits of Mars could survive for a long time but will eventually be swept up.

4.1 Probabilistic neural network

The goal is to train a neural network to predict the stability of the asteroids in the belt. There are four inputs for the neural network, namely the semimajor axis a, eccentricity e, argument of perihelion ω, and mean anomaly M. The only output is '1' or '2', where '1' means temporarily stable, and '2' means unstable.

Here we use the probabilistic neural network (PNN), a supervised non-parametric classification algorithm as opposed to the Gaussian maximum likelihood classifier. The network architecture is shown in Fig. 6. There are four layers of the PNN, namely the input layer, pattern layer, summation layer, and output layer. 98 per cent of the 151 000 data are taken as the training set, while the others are the testing set. The neural network is trained in MATLAB using the function *newpnn*().

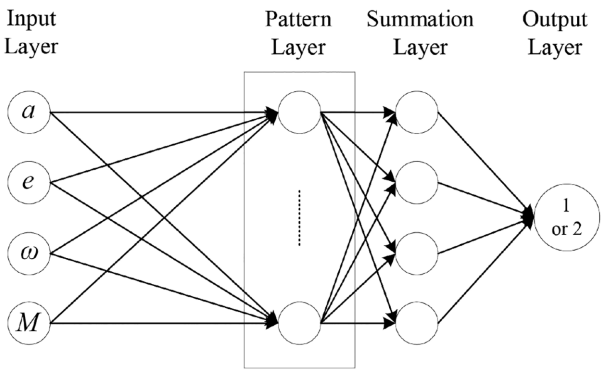

Figure 6. The architecture of the probabilistic neural network.

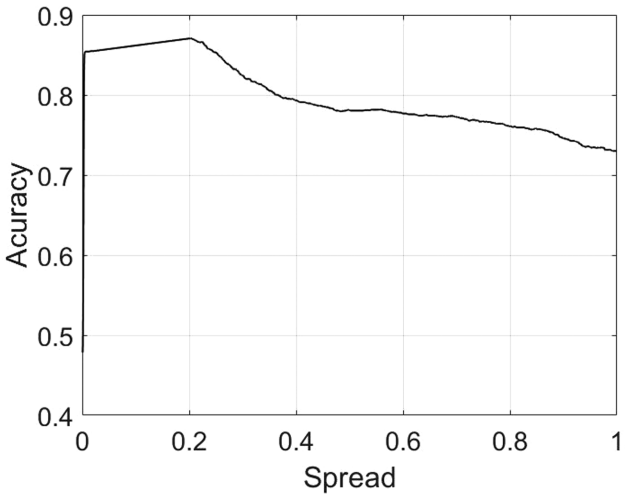

Figure 7. The accuracy of the neural network with different values of *spread*.

The accuracy of the neural network is related to the radial basis function *spread*, which is shown in Fig. 7. Thus *spread* is set to 0.20, and the accuracy of PNN is 87.05 per cent.

If the stability prediction of a particle does not match the numerical result, it is called an error prediction. The error predictions of the testing set are scattered in the *a*-*e* plane, as shown in Fig. 8. Few error predictions are located near the border of the belt in the *a*-*e* plane. Most of the error predictions are located at the positions where the mean motion resonance with Jupiter occurs. To improve the accuracy of predictions, the neural network in the region where the resonance may occur must be trained separately.

4.2 Separately trained neural network

As the error predictions are related to the mean motion resonance, the belt is divided into several parts with respect to the semimajor axis. The ranges of each part are shown in the second and third columns of Table. 3.

Similar to the work in Section 4.1, nine probabilistic neural networks are trained separately in the nine regions listed in Table. 3. The corresponding parameter *spread* and the accuracy of each neural network are shown in columns 4 and 5. The accuracy becomes much better than the result in Section 4.1, and it could be further improved if there are more training data.

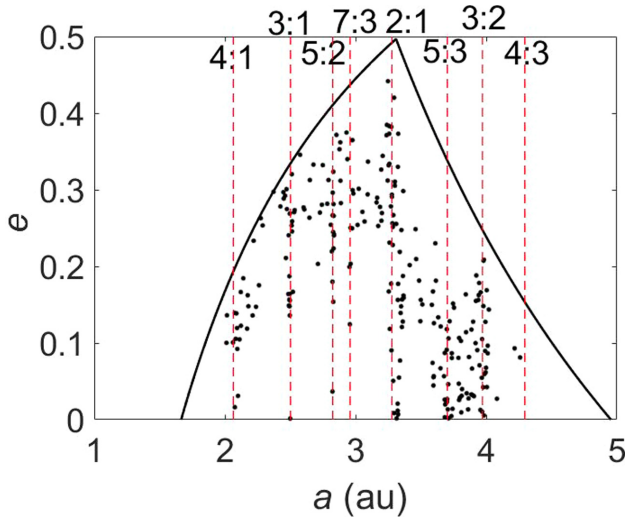

Figure 8. The error predictions of the testing set in the *a*-*e* plane. The vertical dashed lines are the positions of the corresponding resonances. The solid line is the border of the belt in the *a*-*e* plane.

Table 3. The belt is divided into six parts with respect to the semimajor axis. The first column is the mean motion resonance in each part. The last row is the rest regions of the belt. Column 4 gives the value of *spread* of each probabilistic neural network, and column 5 gives their accuracies.

Region	$a_{\min}$ (au)	$a_{\max}$ (au)	*spread*	Accuracy
4/1	2.00	2.10	0.11	1
3/1	2.45	2.55	0.15	0.9271
5/2	2.77	2.87	0.16	0.9467
7/3	2.90	2.99	0.20	0.9355
2/1	3.18	3.38	0.10	0.8631
5/3	3.60	3.80	0.12	0.9386
3/2	3.87	4.07	0.13	0.9183
4/3	4.19	4.39	0.14	0.9676
Rest regions of the belt	–	–	0.06	0.9477

5 APPLICATION OF THE PROBABILISTIC NEURAL NETWORKS

The trained neural networks can be used to predict the stability of the particles based on their initial orbital elements. Of course, the inclinations and the longitudes of the ascending nodes of the particles must be zero. Otherwise, the neural network does not work. The trained neural networks make the prediction faster and easier. There are four dimensions of the initial orbits, so it is difficult to show the stable regions directly. Therefore, the particles' stable regions are projected onto the *a*-*e* plane, where a is the semimajor axis, and e is the eccentricity. To reflect the differences for a particular set of a and e with different ω and M, we make the following definitions:

(1) Absolutely stable region: for a point in the (a, e) plane, if all of the particles at that point with different values of ω and M are region-stable, that point in the *a*-*e* plane is termed an absolutely stable point. All of the absolutely stable points constitute absolutely stable regions.

(2) Absolutely unstable region: for a point in the (a, e) plane, if all of the particles at that point with different values of ω and M are not stable, that point in the *a*-*e* plane is termed an absolutely unstable point. All of the absolutely unstable points constitute absolutely unstable regions.

(3) Mixed region: for a point in the (a, e) plane, if some of the particles at that point are temporarily stable, while others are not, that point in the *a*-*e* plane is termed a mixed point. All of the mixed points constitute the mixed regions.

A large number of particles are generated as follows.

(1) The semimajor axis of the particle in the belt is in the range of $[r_{\min}, r_{\max}]$. Divide the range of the semimajor axis into 1024 equal intervals. The eccentricity, in the range of $[0, e_{\max}]$, is divided into 1024 equal intervals too. Here, $e_{\max}$ is the maximum eccentricity of the asteroids in the belt.

(2) For each group of (a, e), if the orbit with the semimajor axis and eccentricity is located in the belt, the corresponding argument of perigee, in the range of $[0, 2\pi]$, is divided into 20 equal intervals, as is the mean anomaly. Thus, for each combination of (a, e), 400 particles are generated with different ω or M.

Therefore, over 10^8 particles are generated, and every 400 of them can determine the stability of one point in the *a*-*e* plane.

The distribution of these three kinds of regions is shown in Fig. 9. The particles near the border of the belt are probably unstable. The regions show poor stability where the particles are in concordance with 4/1, 3/1, 5/2, 7/3, 2/1 and 5/3 mean motion commensurabilities with Jupiter. There is no absolutely stable region found if $a < 2.1675$ au or $a > 3.8893$ au or $e > 0.2989$. The 4/1, 3/1 and 5/2 mean motion commensurabilities enlarge the absolutely unstable regions, while the 7/3, 2/1, 5/3 and 3/2 ones seem to shrink the regions.

For the particles in the resonant regions: the particles in the black regions will leave the belt; some of the particles in the blue regions will survive; and all the particles in the red regions will survive, no matter if they are resonant with Jupiter or not. Although the temporal stability map can reflect some properties of resonance, the only thing the map can tell is whether the particles will leave the belt or not within the time-scale.

The trained neural networks were also applied to the detected main-belt asteroids. The main-belt asteroid data were downloaded from the Jet Propulsion Laboratory Database (https://ssd.jpl.nasa.gov). Up to 2020 August 31, 938 255 main-belt asteroids had been detected: 20 969 are named inner main-belt asteroids, with $a < 2.0$ au, and 29 600 of them are outer main-belt asteroids, with $a > 3.2$ au. In this work, only four orbital elements are taken into consideration. Thus the inclinations and the longitude ascending nodes of the detected asteroids are assumed to be zero. The predictions are shown in Fig. 10. The red dots denote stable particles, while the black dots denote unstable ones. A total of 827 619 of the asteroids are predicted to be temporarily stable, while 110 636 asteroids are not. This means that about 11.79 per cent of the detected asteroids will leave the belt in the following 8.09×10^6 yr.

Fig. 10 shows that some of the unstable regions are empty today, but that others are not. In this respect, an asteroid's instability only implies that it should leave the belt, but not necessarily permanently. Some of the unstable asteroids leave the belt permanently, such as the asteroids colliding with the Sun or planets. However, many of them will be outside the borders of the belt only temporarily owing to the short periodic perturbations. Once they leave the belt, the planets could clear the planet-crossing objects, but it takes time, especially for Mars. Therefore, some of the temporarily unstable asteroids may actually survive for longer times in the vicinity of the belt's border. That is why some real asteroids are still present in the regions predicted to be temporarily unstable.

In some unstable regions where the asteroids are still present, there may be an active resupply mechanism bringing new objects

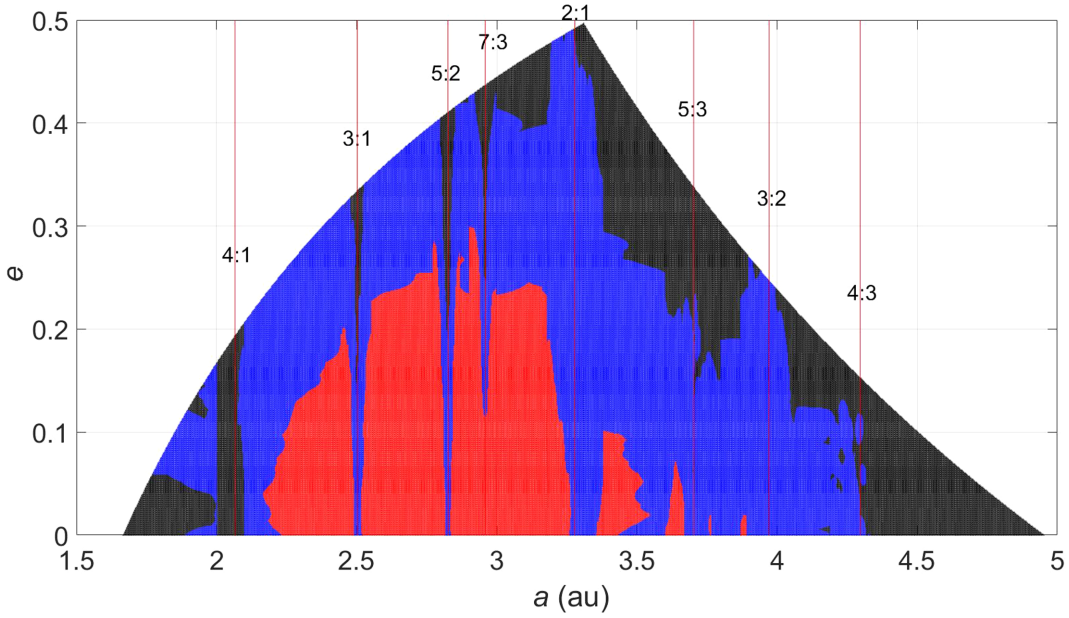

Figure 9. The distribution of the three kinds of regions. The red-coloured regions are the absolutely stable regions, while the blue ones are the mixed regions and the black ones are the absolutely unstable regions.

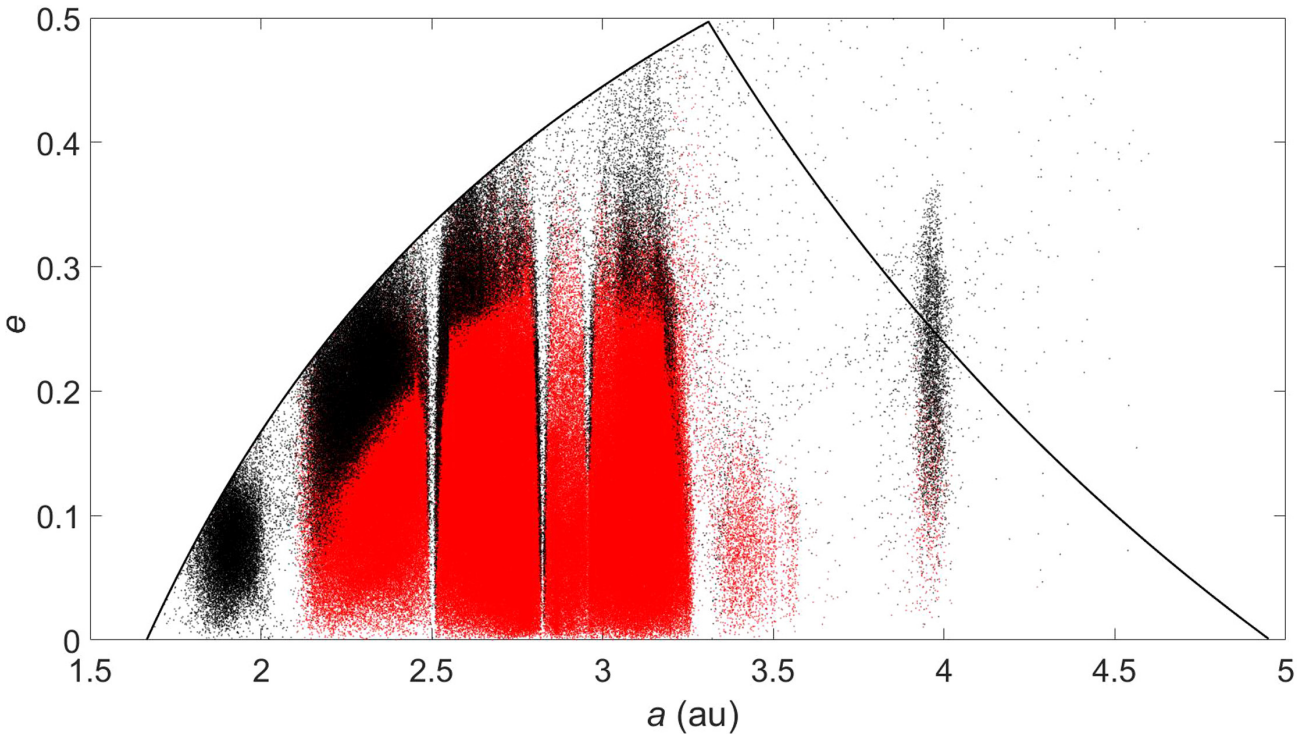

Figure 10. The temporal stability of the detected main-belt asteroids. The red points are temporarily stable, while the black ones are unstable. The solid black line is the border of the belt in the *a*-*e* plane.

inside these areas, for example non-gravitational effects or collisions between the asteroids.

The fraction of unstable objects (11.79 per cent) seems to be very high. However, it should be noted that the fraction of unstable objects is different from the main-belt asteroid escape rate. The temporarily unstable asteroids could survive for a time longer than about 8 Myr, as explained above. The 'unstable region' does not mean that the asteroids in that region will be swept, but that the asteroids will leave the belt. They may come back and then repeat the process. In addition, 1776 asteroids are initially located outside the borders of the belt, as shown in Fig. 10, and therefore these objects are by definition temporarily unstable. Still, even some of them could survive. This explains the large fraction of 11.79 per cent of the asteroids found to be unstable in our analysis.

Finally, it should be noted that the inclinations and the longitudes of the ascending nodes of the asteroids are assumed to be zero. That is an additional reason why the prediction did not match the real situation.

6 CONCLUSIONS

This work has studied the temporal stability of the main-belt asteroids. The fitted function of the distribution of instability time has been obtained, and a new method has been presented to choose the time-scale of numerical integration based on the ratio of instability. The method can be used in other problems to determine the time-scale of the numerical simulation.

In our work, the time-scale was 8.09×10^6 yr, at which time the ratio of instability reaches 0.95. With better computational ability, a longer time-scale with a greater ratio of instability could be chosen.

The numerical integration was parallel-computed using a computer with 20 cores. It took a long time, namely over six months. The results of the integration give the stability of 151 000 particles. Nine probabilistic neural networks were trained separately based on the data and show a good performance for predicting the stability of the particles. Note that the trained neural network can only tell the stability of a particle within 8.09×10^6 yr.

A map of the stable region in the *a*-*e* plane was derived after the simulation of over 10^8 particles using the trained neural networks. It depicts three kinds of regions: the absolutely stable region, the absolutely unstable region, and the mixed region. This proves an advantage of the method, namely that with no integration, the stability of a particle can be determined immediately.

The trained neural networks were also applied to the detected main-belt asteroids. As their inclinations and the longitudes of the ascending nodes were assumed to be zero, the neural networks may only provide a reasonable prediction compared with the real situation.

The limitations of the approach need to be pointed out. First, to reduce the computational cost, here we have studied only the simplified situation, where the initial orbital inclinations and the longitudes of the ascending nodes of the particles are set to zero. The method as a whole still works if there is no restriction on the initial orbits of the particles. In that case, the distribution of instability time needs to be fitted again. The following steps are similar to the planar case shown in this work, but many more particles need to be integrated to train the neural network.

Secondly, the neural networks can only tell whether an asteroid is temporarily stable on this time-scale. The instability time of each asteroid is still unknown.

Thirdly, despite being reasonably reliable, the predictions of the PNN are less accurate than the numerical integrations. Therefore, the results obtained using the PNN could be useful as a fast preliminary indication of stability. A much more in-depth analysis is needed to fully assess the dynamical stability of individual asteroids.

ACKNOWLEDGEMENTS

This work was supported by the National Natural Science Foundation of China (grant nos 11772167 and 11822205).

DATA AVAILABILITY

The data underlying this article will be shared on reasonable request to the corresponding author.

REFERENCES

Alessio M., Dario I., 2018, Astrodynamics, 2, 249
Bottke W. F., Durda D. D., Nesvorný D., Jedicke R., Morbidelli A., Vokrouhlický D., Levison H. F., 2005, Icarus, 179, 63
Bottke W. F., Vokrouhlický D., Rubincam D. P., Nesvorný D., 2006, Annu. Rev. Earth Planet. Sci., 34, 157
Carruba V., Vokrouhlický D., Novaković B., 2018, Planetary and Space Science, 157, 72
Chambers J., Migliorini F., 1997, Bull. Am. Astron. Soc., 29, 1024
Chambers J., Wetherill G., Boss A., 1996, Icarus, 119, 261
Clement M., Kaib N. A., Raymond S. N., Walsh K. J., 2018, Icarus, 311, 340
Clement M. S., Morbidelli A., Raymond S. N., Kaib N. A., 2019, MNRAS, 492, L56
Deienno R., Gomes R. S., Walsh K. J., Morbidelli A., Nesvorný D., 2016, Icarus, 272, 114
Delbo' M., dell'Oro A., Harris A. W., Mottola S., Mueller M., 2007, Icarus, 190, 236
Donnison J. R., Mikulskis D. F., 1992, MNRAS, 254, 21
Donnison J. R., Mikulskis D. F., 1994, MNRAS, 266, 25
Duncan M. J., Lissauer J. J., 1997, Icarus, 125, 1
Faber P., Quillen A. C., 2007, MNRAS, 382, 1823
Gladman B. J. et al., 1997, Science, 277, 197
Granvik M., Morbidelli A., Vokrouhlický D., Bottke W. F., Nesvorný D., Jedicke R., 2017, A&A, 598, A52
Harrington R. S., 1972, Celest. Mech., 6, 322
Holman M., Wiegert P., 1996, AJ, 28, 1113
Hsieh H. H., Novaković B., Walsh K. J., Schorghofer N., 2020, AJ, 159, 179
Jopek T. J., 2020, MNRAS, 494, 680
Malhotra R., Wang X., 2016, MNRAS, 465, 4381
Milani A., Kneevi Z., Novaković B., Cellino A., 2010, Icarus, 207, 769
Minton D. A., Malhotra R., 2009, Nature, 457, 1109
Minton D. A., Malhotra R., 2010, Icarus, 207, 744
Minton D. A., Malhotra R., 2011, ApJ, 732, 205
Moons M., 1997, Review of the Dynamics in the Kirkwood Gaps. Springer, Dordrecht, Netherlands
Novaković B., Maurel C., Tsirvoulis G., Knežević Z., 2015, ApJ, 807, L5
Obertas A., Van Laerhoven C., Tamayo D., 2017, Icarus, 293, 52
Roig F., Nesvorný D., 2015, AJ, 150, 186
Smirnov E. A., Dovgalev I. S., Popova E. A., 2018, Icarus, 304, 24
Smith A. W., Lissauer J. J., 2009, Icarus, 201, 381
Tamayo D. et al., 2016, ApJ, 832, L22
Todorović N., Novaković B., 2015, MNRAS, 451, 1637
Wisdom J., 1982, AJ, 87, 577
Wisdom J., 1983, Icarus, 63, 272
Yan X., Li J., 2019, Sci. Sinica (Phys., Mech. Astron.), 49, 084511

This paper has been typeset from a TEX/LATEX file prepared by the author.